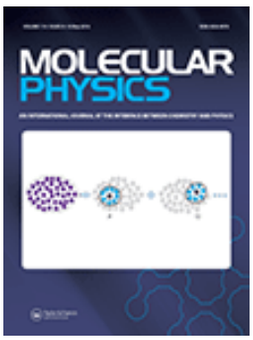

Taylor & Francis
Taylor & Francis Group

Molecular Physics

An International Journal at the Interface Between Chemistry and Physics

ISSN: 0026-8976 (Print) 1362-3028 (Online) Journal homepage: http://www.tandfonline.com/loi/tmph20

MOlecular MAterials Property Prediction Package (MOMAP) 1.0: a software package for predicting the luminescent properties and mobility of organic functional materials

Yingli Niu, Wenqiang Li, Qian Peng, Hua Geng, Yuanping Yi, Linjun Wang, Guangjun Nan, Dong Wang & Zhigang Shuai

To cite this article: Yingli Niu, Wenqiang Li, Qian Peng, Hua Geng, Yuanping Yi, Linjun Wang, Guangjun Nan, Dong Wang & Zhigang Shuai (2018): MOlecular MAterials Property Prediction Package (MOMAP) 1.0: a software package for predicting the luminescent properties and mobility of organic functional materials, Molecular Physics, DOI: 10.1080/00268976.2017.1402966

To link to this article: https://doi.org/10.1080/00268976.2017.1402966

Published online: 06 Feb 2018.

MOLECULAR PHYSICS, 2018
https://doi.org/10.1080/00268976.2017.1402966

Taylor & Francis
Taylor & Francis Group

MOLECULAR PHYSICS IN CHINA

MOlecular MAterials Property Prediction Package (MOMAP) 1.0: a software package for predicting the luminescent properties and mobility of organic functional materials

Yingli Niu[a,*], Wenqiang Li[b,*], Qian Peng[c], Hua Geng[d], Yuanping Yi[c], Linjun Wang[e], Guangjun Nan[f], Dong Wang[b] and Zhigang Shuai[b]

[a]Department of Physics, School of Science, Beijing Jiaotong University, Beijing, China; [b]Department of Chemistry, Tsinghua University, Beijing, China; [c]Key Laboratory of Organic Solids, Institute of Chemistry, Chinese Academy of Sciences, Beijing, China; [d]Department of Chemistry, Capital Normal University, Beijing, China; [e]Department of Chemistry, Zhejiang University, Hangzhou, China; [f]School of Chemistry and Chemical Engineering, Harbin Institute of Technology, Harbin, China

ABSTRACT

MOlecular MAterials Property Prediction Package (MOMAP) is a software toolkit for molecular materials property prediction. It focuses on luminescent properties and charge mobility properties. This article contains a brief descriptive introduction of key features, theoretical models and algorithms of the software, together with examples that illustrate the performance. First, we present the theoretical models and algorithms for molecular luminescent properties calculation, which includes the excited-state radiative/non-radiative decay rate constant and the optical spectra. Then, a multi-scale simulation approach and its algorithm for the molecular charge mobility are described. This approach is based on hopping model and combines with Kinetic Monte Carlo and molecular dynamics simulations, and it is especially applicable for describing a large category of organic semiconductors, whose inter-molecular electronic coupling is much smaller than intra-molecular charge reorganisation energy.

ARTICLE HISTORY
Received 29 September 2017
Accepted 6 November 2017

KEYWORDS
Molecular materials; luminescence; charge transport; first principle

1. Introduction

Computational design of advanced materials has become one of the most important challenges in academia and industry, as emphasised in the known 'Material Genome Initiative (MGI) for global competitiveness' [1]. Organic opto-electronic functional materials have attracted great attentions owing to their potential applications in promising solid-state photo-electronic devices, such as organic light emitting diodes (OLEDs), field effect transistors, sensors, solar cells and so on. Our initial intention was to investigate the fluorescence and phosphorescence spectra and quantum efficiency and carrier mobility for organic functional materials. While spectra calculation modules can be found in a number of quantum chemistry packages, evaluations for other key molecular parameters were not available a decade ago. Especially, the AIE (aggregation-induced emission) phenomena was discovered by Tang *et al.* [2], arousing strong interests, where the non-radiative decay process suppressed by aggregation has been identified to be the essential cause, though several other propositions have been postulated. The excited state decay process has long been a challenging issue for theoretical chemistry. We noted that the time scale for fluorescence for OLEDs materials is around 10 ns and for phosphorescence ranging micro- to milli-seconds. Typical compound for OLEDs possesses ~50 atoms. Excited

CONTACT Qian Peng qpeng@iccas.ac.cn; Zhigang Shuai zgshuai@tsinghua.edu.cn
*These authors contribute equally.

state dynamics for such a complex system is simply impossible at full quantum level so far.

We thus had turned to Fermi Golden Rule taking both non-adiabatic coupling [3] and spin-orbit coupling [4] as perturbation. When formulating in a time-dependent fully analytic vibration correlation function formalism, it turns out that the evaluated rates are in satisfactory agreement with experiments [5]. Such formalism combining with quantum mechanics / molecular mechanics (QM/MM) model has been successfully applied to quantitative assessment of the AIE effect, such as how the molecular aggregation suppressing the non-radiative decay [6]. A number of plausible probing approaches have been proposed theoretically to verify the suggested mechanism [7,8]. The formalism has also been applied to evaluate the phosphorescence efficiency for organometallic compounds [9] and for molecular design of highly efficient deep blue emitter [10]. In addition, thermally activated delayed fluorescence (TADF) phenomena have been widely employed for molecular design for highly efficient electroluminescent materials [11]. In such system, the electro-pumped carriers form excitons, and the statistical 75% triplets can be easily converted to emissive singlets, enhancing the overall quantum efficiency. The relevant internal conversion and intersystem crossing rates have been evaluated by our method [12,13].

Carrier mobility is an essential physical parameter for opto-electronics. As far as organic semiconductors are concerned, the semi-classical Marcus theory has been first proposed by Brédas *et al.*, assuming localised charge hopping mechanism [14]. Later, a number of developments have been proposed along this line such as Kinetic Monte Carlo for evaluating charge diffusion constant [15], quantum nuclear tunnelling (QNT) model [16] and deformation potential theory for band-like behaviour [17]. Note that the evaluation of carrier mobility is parameter-free, rendering a first-principles prediction for such an important quantity.

Here, we introduce MOMAP, standing for MOlecular MAterials Property Prediction Package, as a useful tool for molecular materials' properties prediction. Now the released version 1.0 of MOMAP focuses on luminescent properties and charge mobility properties. By using MOMAP, we have investigated the conversion and decay processes of TADF molecules [12], the mechanism of the AIE phenomenon [8,18,19], the nuclear quantum tunnelling effects in organic semiconductors [20], the influence of alkyl side-chain length on the organic materials' carrier mobility [21] and so on. According to our statistics, MOMAP has been downloaded over 2600 times before its commercialisation. In addition, it has been applied to the calculations of the internal conversion rate of Cu_n(n = 3,6 and 9) and H_2/Cu_3 by Chiodo and Mineva [22], the fluorescent radiative rate constants of meta-organic framework by Hao *et al.* [23], the radiative and non-radiative rate constants of the aminoanthracene derivatives by Escudero [24], the non-radiation decay rate constants by Lin *et al.* [13] and so on.

Here, the program's summaries are as follows:

Program summary:
Program title: MOMAP
Version Number: V1.0
Chinese Software Copyright Registration Number: 2017SR072448
Program released URL: www.momap.net.cn
Number of lines in distributed program: 52 582
Distribution format: tar.gz
Programming language: Fortran, Linux Shell Script
Computer: all Linux based workstation, supercomputer and Mac OS
Has the code been parallelized?: Code is parallelized by MPICH, OPENMPI and IMPI

Target of this version of MOMAP: optical spectra (absorption, fluorescence, phosphorescence) and rate constants (radiative, internal conversion, intersystem crossing) of polyatomic molecules. The transfer integral, reorganisation energy of neutral and charged molecules, charge transfer rate (full-quantum or Marcus-type) between two molecules and the charge mobility within a molecular crystal, see Figure 1.

Method employed in this version of MOMAP: Based on the electronic structure provided by quantum chemistry package, a thermal vibrational correlation function (TVCF) formalism is employed to luminescent principle [3,4,25–28]. This formalism is derived from Fermis' golden rule and harmonic oscillator model, as well as considering mode-mixing (Duschinsky rotation effect) and the coordinate-dependent transition dipole (Herzberg–Teller effect). It is an analytical time-integrated rate formalism, which can be solved by fast-Fourier transformation technique, making the program very efficient. As for charge mobility simulation [29–34], site energy correction method has been employed to evaluate intermolecular electronic coupling (transfer integral). QNT effect was taken into account through full quantum charge transfer rate formula. Kinetic Monte Carlo was adopted to simulate charge diffusion in bulk material. The combination of quantum charge treatment and Kinetic Monte Carlo provides an efficient strategy to simulate charge diffusion in bulk material.

Additional comments: the simulated luminescent principle may not agree with the experiments for organic molecule with anharmonic behaviour, since the harmonic oscillator model is employed. The program

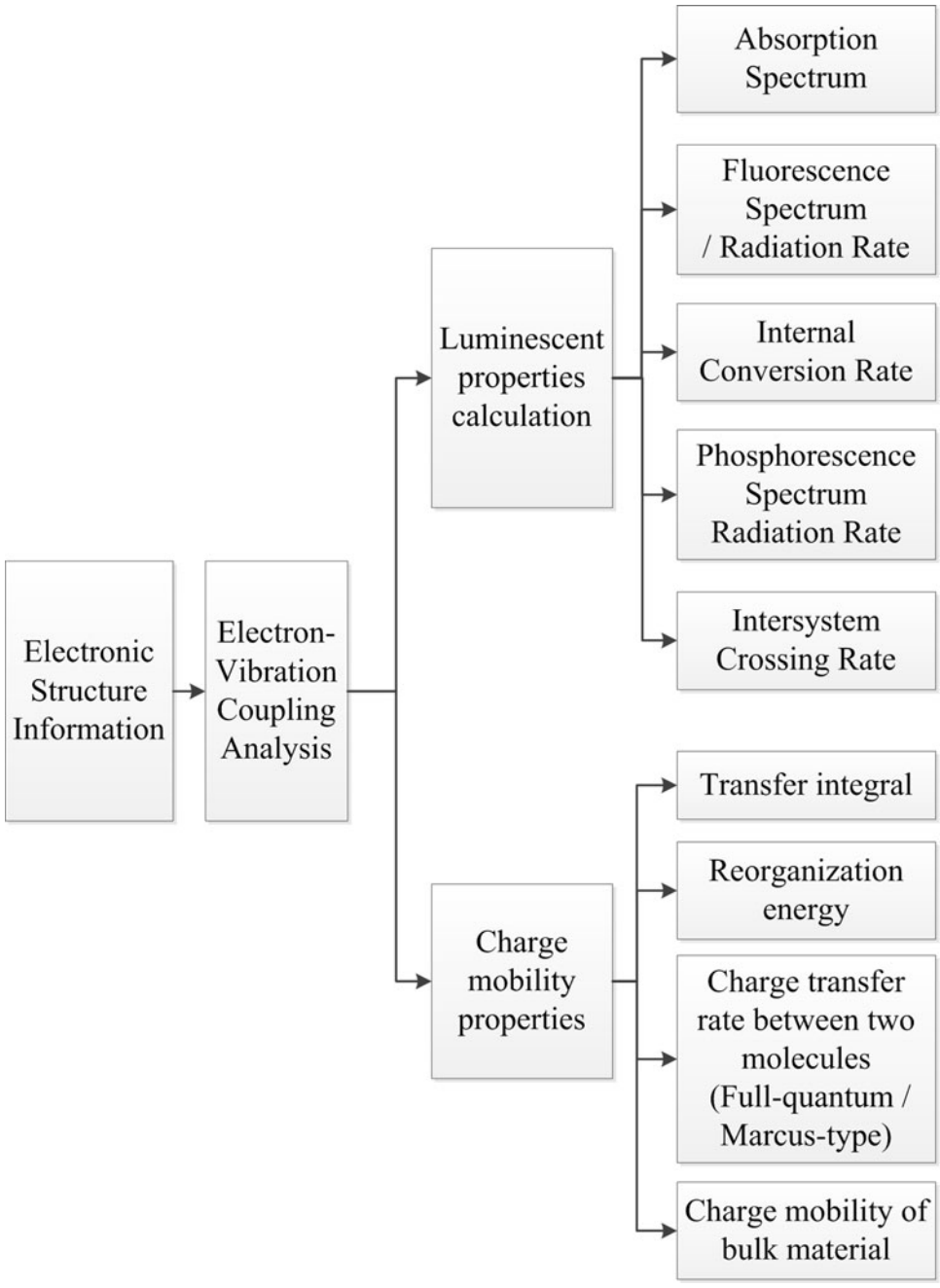

Figure 1. Function structure chart of MOMAP V1.0.

needs an initial packing structure for the charge mobility simulation.

2. Quantitative prediction of molecular photophysical parameters

2.1. Fluorescence spectrum and radiative decay rate

Based on the Fermi Golden Rule and Born–Oppenheimer approximation, the absorption cross section and differential radiative rate can be expressed as [28]

$$\sigma_{\text{abs}}(\omega, T) = \frac{4\pi^2\omega}{3\hbar c} \times \sum_{v_i, v_f} P_{iv_i}(T) \left|\left\langle \Theta_{f,v_f} \left|\boldsymbol{\mu}_{fi}\right| \Theta_{i,v_i}\right\rangle\right|^2 \delta\left(\omega - \omega_{fv_f,iv_i}\right), \tag{1}$$

$$\sigma_{\text{emi}}(\omega, T) = \frac{4\omega^3}{3\hbar c^3} \times \sum_{v_i, v_f} P_{iv_i}(T) \left|\left\langle \Theta_{f,v_f} \left|\boldsymbol{\mu}_{fi}\right| \Theta_{i,v_i}\right\rangle\right|^2 \delta\left(\omega_{iv_i,fv_f} - \omega\right). \tag{2}$$

Here, $P_{iv_i}(T)$ is the Boltzmann distribution of the vibration manifolds in the initial state. $\boldsymbol{\mu}_{fi} = \langle \Phi_f | \hat{\boldsymbol{\mu}} | \Phi_i \rangle$ is the electric transition dipole moment between the initial state i and final state f. v_i/v_f is vibrational quantum number of state i/f, ω is the frequency, $\omega_{iv_i, fv_f} = \omega_{fv_f} - \omega_{iv_i}$, respectively. Considering both Duschinsky effect and Herzberg–Tell effect, the Equations (1) and (2) can be expressed in the framework of TVCF and solved analytically by Gaussian integrations. Taking the absorption cross section as an example, Equation (1) can be derived as

$$\sigma_{\text{abs}}^{\text{FC}}(\omega, T) = \frac{2\pi\omega}{3\hbar^2 \text{c}} |\boldsymbol{\mu}_0|^2 \int_{-\infty}^{\infty} \text{d}t \text{e}^{i(\omega-\omega_{fi})t} \left[Z_i^{-1} \rho_{\text{abs},0}^{\text{FC}}(t, T) \right], \quad (3)$$

$$\sigma_{\text{abs}}^{\text{FC/HT}}(\omega, T) = \frac{2\pi\omega}{3\hbar^2 \text{c}} \int_{-\infty}^{\infty} \text{d}t \text{e}^{i(\omega-\omega_{fi})t} \times \left[Z_i^{-1} \sum_k \boldsymbol{\mu}_0 \cdot \boldsymbol{\mu}_k \rho_{\text{abs},k}^{\text{FC/HT}}(t, T) \right], \quad (4)$$

$$\sigma_{\text{abs}}^{\text{HT}}(\omega, T) = \frac{2\pi\omega}{3\hbar^2 \text{c}} \int_{-\infty}^{\infty} \text{d}t \text{e}^{i(\omega-\omega_{fi})t} \times \left[Z_i^{-1} \sum_{k,l} \boldsymbol{\mu}_k \cdot \boldsymbol{\mu}_l \rho_{\text{abs},kl}^{\text{HT}}(t, T) \right], \quad (5)$$

where

$$\rho_{\text{abs},0}^{\text{FC}}(t, T) = \sqrt{\frac{\det\left[\mathbf{a}_f \mathbf{a}_i\right]}{\det\left[\mathbf{K}\right]}} \exp\left\{ -\frac{i}{\hbar} \left[\frac{1}{2} \underline{F}^T \mathbf{K} \underline{F} - \underline{D}^T \mathbf{E} \underline{D} \right] \right\}, \quad (6)$$

$$\rho_{\text{abs},k}^{\text{FC/HT}}(t, T) = -\rho_{\text{abs},0}^{\text{FC}}(t, T) \left\{ \underline{H}_k^{\text{FC/HT}} \mathbf{K}^{-1} \underline{F} \right\}, \quad (7)$$

$$\rho_{\text{abs},kl}^{\text{HT}}(t, T) = \rho_{\text{abs},0}^{\text{FC}}(t, T) \times \left\{ i\hbar \text{Tr}\left[\mathbf{G}_{lk}^{\text{HT}} \mathbf{K}^{-1} \right] + \left(\mathbf{K}^{-1} \underline{F} \right)^T \mathbf{G}_{lk}^{\text{HT}} \left(\mathbf{K}^{-1} \underline{F} \right) \right\}. \quad (8)$$

Here,

$$\mathbf{K} = \begin{bmatrix} \mathbf{B} & -\mathbf{A} \\ -\mathbf{A} & \mathbf{B} \end{bmatrix}_{2N \times 2N}, \quad (9)$$

$$\underline{F} = \left[\underline{D}^{\text{T}} \mathbf{E} \mathbf{S} \ \underline{D}^{\text{T}} \mathbf{E} \mathbf{S} \right]_{1 \times 2N}^{\text{T}}, \quad (10)$$

$$\underline{H}_k^{\text{FC/HT}} = [0_1 \cdots 1_k \cdots 0_{2N}]_{1 \times 2N}^{\text{T}}, \quad (11)$$

$$\mathbf{G}_{kl}^{\text{HT}} = \begin{bmatrix} 0_{11} & 0_{12} & \cdots & 0_{1N+l} & \cdots \\ 0_{21} & 0_{22} & \cdots & 0_{2N+l} & \cdots \\ \cdots & \cdots & \cdots & \cdots & \cdots \\ 0_{k1} & 0_{k2} & \cdots & 1_{kN+l} & \cdots \\ \cdots & \cdots & \cdots & \cdots & \cdots \end{bmatrix}_{2N \times 2N}, \quad (12)$$

$$\mathbf{A} \equiv \mathbf{a}_f + \mathbf{S}^{\text{T}} \mathbf{a}_i \mathbf{S}, \quad (13)$$

$$\mathbf{B} \equiv \mathbf{b}_f + \mathbf{S}^{\text{T}} \mathbf{b}_i \mathbf{S}, \quad (14)$$

$$\mathbf{E} \equiv \mathbf{b}_i - \mathbf{a}_i, \quad (15)$$

$\mathbf{a}_{i/f}$ and $\mathbf{b}_{i/f}$ are diagonal with elements $a_{i/f,k}(\tau_{i/f}) = \omega_{i/f,k}/\sin(\hbar\omega_{i/f,k}\tau_{i/f})$ and $b_{i/f,k}(\tau_{i/f}) = \omega_{i/f,k}/\tan(\hbar\omega_{i/f,k}\tau_{i/f})$, $\omega_{i/f,k}$ is kth normal mode vibration frequency of the initial/final state respectively. Defining

$$\tilde{\mu}_{\text{abs}}^2(t, T) = |\vec{\mu}_0|^2 - \sum_k \vec{\mu}_0 \cdot \vec{\mu}_k \left[\left(\underline{H}_k^{\text{FC/HT}} \right)^{\text{T}} \mathbf{K}^{-1} \underline{F} \right] + \sum_{kl} \vec{\mu}_k \cdot \vec{\mu}_l \left[i\hbar \text{Tr}\left[\mathbf{G}_{kl}^{\text{HT}} \mathbf{K}^{-1} \right] + \left(\mathbf{K}^{-1} \underline{F} \right)^{\text{T}} \mathbf{G}_{kl}^{\text{HT}} \left(\mathbf{K}^{-1} \underline{F} \right) \right]. \quad (16)$$

Then, the total absorption spectrum formalism becomes

$$\sigma_{\text{abs}}(\omega) = \frac{2\pi\omega}{3\hbar^2 \text{c}} \int_{-\infty}^{\infty} \text{d}t \text{e}^{i(\omega-\omega_{fi})t} Z_i^{-1} \tilde{\boldsymbol{\mu}}_{\text{abs}}^2(t, T) \rho_{\text{abs},0}^{\text{FC}}(t, T). \quad (17)$$

Similarly, the fluorescence spectrum is

$$\sigma_{\text{fluo}}(\omega) = \frac{2\omega^3}{3\pi\hbar \text{c}^3} \int_{-\infty}^{\infty} \text{d}t \text{e}^{-i(\omega-\omega_{if})t} Z_i^{-1} \tilde{\boldsymbol{\mu}}_{\text{fluo}}^2(t, T) \rho_{\text{fluo},0}^{\text{FC}}(t, T). \quad (18)$$

The radiative rate can be obtained from the integration of Equation (18):

$$k_r = \int_0^{\infty} \sigma_{\text{fluo}}(\omega) \text{d}\omega. \quad (19)$$

2.2. Non-radiative decay rate

As for non-radiative decay, applying the second-order perturbation approximation, the rate constant reads [28]

$$k_{f \leftarrow i} = \frac{2\pi}{\hbar} \sum_{v_i, v_f} P_{iv_i} \left| H'_{fv_f, iv_i} + \sum_{n, v_n} \frac{H'_{fv_f, nv_n} H'_{nv_n, iv_i}}{E_{iv_i} - E_{nv_n}} \right|^2 \delta \times \left(E_{iv_i} - E_{fv_f} \right). \quad (20)$$

Here, v_i/v_f is vibrational quantum number of the initial state (i) final state (f) and H' denotes the interaction

between two different BO states, which reads

$$\hat{H}'\Psi_{iv_i} = \hat{H}^{\mathrm{NA}}\Phi_i(\mathbf{r};\mathbf{Q})\,\Theta_{iv_i}(\mathbf{Q}) + \hat{H}^{\mathrm{SO}}\Phi_i(\mathbf{r};\mathbf{Q})\,\Theta_{iv_i}(\mathbf{Q}), \quad (21)$$

where $\hat{H}^{\mathrm{NA}}$ is the non-adiabatic coupling operator, $\hat{H}^{\mathrm{SO}}$ is the spin-orbital coupling operator. $\mathbf{r}$ and $\mathbf{Q}$ are the electronic and nuclear normal mode coordinates. Based on Fermi Golden rule and Condon approximation, we get

$$k_{\mathrm{ic}} = \sum_{k,l}\frac{1}{\hbar^2}R_{kl}\int_{-\infty}^{\infty}\mathrm{d}t\mathrm{e}^{i\omega_{if}t}Z_i^{-1}\rho_{\mathrm{ic},kl}, \quad (22)$$

where

$$\rho_{\mathrm{ic},kl} = \sqrt{\frac{\det\left[\mathbf{a}_f\mathbf{a}_i\right]}{\det\left[\mathbf{K}\right]}}\exp\left\{-\frac{i}{\hbar}\left[\frac{1}{2}\underline{F}^T\mathbf{K}^{-1}\underline{F} - \underline{D}^T\mathbf{E}\underline{D}\right]\right\} \times\left\{i\hbar\mathrm{Tr}\left[\mathbf{G}_{kl}^{\mathrm{IC}}\mathbf{K}^{-1}\right] + \left(\mathbf{K}^{-1}\underline{F}\right)^T\mathbf{G}_{kl}^{\mathrm{IC}}\left(\mathbf{K}^{-1}\underline{F}\right) - \underline{H}_{kl}^{\mathrm{IC}}\mathbf{K}^{-1}\underline{F}\right\}. \quad (23)$$

The definitions of matrices $\mathbf{K}$, and vectors $\underline{F}$, have been given in Section 2.1. The definition of G_{kl}^{IC} and H_{kl}^{IC} can be found in Ref. [28].

2.3. Phosphorescence spectrum and intersystem crossing rate

Phosphorescence is originated from spin-orbit coupling. By applying the perturbation theory, we express the perturbed singlet and triplet states ($|\mathrm{S}'\rangle$and $|\mathrm{T}'\rangle$) as [4]

$$|S'\rangle = |S\rangle + \sum_n\sum_{\kappa'=1}^{3}\frac{\langle{}^3n_{\kappa'}|\hat{H}^{\mathrm{SO}}|S\rangle}{{}^1E_S^0 - {}^3E_n^0}|{}^3n_{\kappa'}\rangle, \quad (24)$$

$$|T'_\kappa\rangle = |T_\kappa\rangle + \sum_k\frac{\langle{}^1k|\hat{H}^{\mathrm{SO}}|T_\kappa\rangle}{{}^3E_T^0 - {}^1E_k^0}|{}^1k\rangle. \quad (25)$$

Here, the $|\mathrm{S}\rangle$ and $|\mathrm{T}\rangle$ are pure singlet and triplet states, $\hat{H}^{\mathrm{SO}}$ is the spin-orbital coupling operator. Thus, the transition dipole moment recasts

$$\boldsymbol{\mu}_{ST_\kappa} = \sum_k^{\{\mathrm{singlets}\}}\frac{\langle S|\boldsymbol{\mu}|{}^1k\rangle\langle{}^1k|\hat{H}^{\mathrm{SO}}|T_\kappa\rangle}{{}^3E_T^0 - {}^1E_k^0} + \sum_n^{\{\mathrm{triplets}\}}\sum_{\kappa'=1}^{3}\frac{\langle S|\hat{H}^{\mathrm{SO}}|{}^3n_{\kappa'}\rangle\langle{}^3n_{\kappa'}|\boldsymbol{\mu}|T_\kappa\rangle}{{}^1E_S^0 - {}^3E_n^0}, \quad (26)$$

where κ is the magnetic quantum number. N and k are the intermediate triplet and singlet electronic states, respectively. Applying the Franck–Condon approximation, the phosphorescence spectrum can be expressed as

$$\sigma_{\mathrm{ph}}(\omega,T) = \frac{4\omega^3}{3\hbar\mathrm{c}^3}\sum_{v_i,v_f}P_{iv_i}(T)\left|\langle\Theta_{f,v_f}|\boldsymbol{\mu}_{\mathrm{ST}}|\Theta_{i,v_i}\rangle\right|^2 \times\delta\left(\omega_{iv_i,fv_f} - \omega\right). \quad (27)$$

Applying Fourier transformation, Equation (27) can be rewritten as

$$\sigma_{\mathrm{ph}}(\omega) = \frac{2\omega^3\left|\mu_{\mathrm{ST}}\right|^2}{3\pi\hbar\mathrm{c}^3}\int_{-\infty}^{\infty}\mathrm{d}t\mathrm{e}^{-i\left(\omega-\omega_{if}\right)t}Z_i^{-1}\rho_{\mathrm{ph},0}^{\mathrm{FC}}(t,T) \quad (28)$$

$\rho_{\mathrm{ph},0}^{\mathrm{FC}}$ is simply the Franck–Condon factor like Equation (6), see Ref [4].

Now, we consider the intersystem crossing process, from T_1 to S_0. Expanding Equation (20), we obtain

$$k_{\mathrm{isc}} = k_{\mathrm{isc}}^{(0)} + k_{\mathrm{isc}}^{(1)} + k_{\mathrm{isc}}^{(2)}, \quad (29)$$

where

$$k_{\mathrm{isc}}^{(0)} = \frac{2\pi}{\hbar}\sum_{v_i,v_f}P_{iv_i}\left|H'_{fv_f,iv_i}\right|^2\delta\left(E_{iv_i} - E_{fv_f}\right), \quad (30)$$

$$k_{\mathrm{isc}}^{(1)} = \frac{2\pi}{\hbar}\sum_{v_i,v_f}P_{iv_i}\cdot 2\mathrm{Re}\left(H'_{fv_f,iv_i}\sum_{n,v_n}\frac{H'_{iv_i,nv_n}H'_{nv_n,fv_f}}{E_{iv_i} - E_{nv_n}}\right) \times\delta\left(E_{iv_i} - E_{fv_f}\right), \quad (31)$$

$$k_{\mathrm{isc}}^{(2)} = \frac{2\pi}{\hbar}\sum_{v_i,v_f}P_{iv_i}\left|\sum_{n,v_n}\frac{H'_{fv_f,nv_n}H'_{nv_n,iv_i}}{E_{iv_i} - E_{nv_n}}\right|^2\delta\left(E_{iv_i} - E_{fv_f}\right). \quad (32)$$

Thus, the vibration correlation functions can be expressed as

$$k_{\mathrm{isc}}^{(0)} = \frac{1}{\hbar^2}R_{fi}^{\mathrm{isc}}\int_{-\infty}^{\infty}\mathrm{d}t\mathrm{e}^{i\omega_{if}t}Z_i^{-1}\rho_{\mathrm{isc}}^{(0)}(t,T), \quad (33)$$

$$k_{\mathrm{isc}}^{(1)} = \mathrm{Re}\left[\frac{1}{\hbar^2}\int_{-\infty}^{\infty}\mathrm{d}t\mathrm{e}^{i\omega_{if}t}Z_i^{-1}\sum_k 2R_{fi,k}^{\mathrm{isc}}\rho_{\mathrm{isc},k}^{(1)}(t,T)\right], \quad (34)$$

$$k_{\mathrm{isc}}^{(2)} = \frac{1}{\hbar^2}\int_{-\infty}^{\infty}\mathrm{d}t\mathrm{e}^{i\omega_{if}t}Z_i^{-1}\sum_{k,l}R_{fi,kl}^{\mathrm{isc}}\rho_{\mathrm{isc},kl}^{(2)}(t,T). \quad (35)$$

It is noted that $\rho_{\mathrm{isc}}^{(0)}$ ($\rho_{\mathrm{isc}}^{(2)}$) is the same as Equation (6) (and Equation (23)) except the definition of initial and final state, $\rho_{\mathrm{isc}}^{(1)}$can be solved similarly, see Ref. [4],

$$\rho_{\mathrm{isc},k}^{(1)}(t,T) = -\underline{H}_k^{\mathrm{T}}\mathbf{K}^{-1}\underline{F}\sqrt{\frac{\det\left[\mathbf{a}_f\mathbf{a}_i\right]}{\det\left[\mathbf{K}\right]}} \times\exp\left\{\frac{i}{\hbar}\left[-\frac{1}{2}\underline{F}^{\mathrm{T}}\mathbf{K}^{-1}\underline{F} + \underline{D}^{\mathrm{T}}\mathbf{E}\underline{D}\right]\right\} \quad (36)$$

The definitions of matrices $\mathbf{K}$, $\mathbf{E}$ and vectors $\underline{F}$ are given in Section 2.1.

2.4. Algorithm

The program algorithms of luminescent properties are listed as follows, including the electronic vibrational coupling analysis part; the absorption, fluorescence spectrum and radiative rate constant calculation part; internal conversion rate constant calculation part; phosphorescence spectrum, radiative rateconstant, intersystem crossing rate constant calculation part.

(1) Electronic vibrational coupling analysis (evc) part

This procedure is for the displacement and Duschinsky rotation matrix
m: molecular mass
x_g: molecular coordinate of ground state
x_e: molecular coordinate of excited state
fc_g: molecular force constant of ground state
fc_e: molecular force constant of excited state
nacme: non-adiabatic coupling matrix element
dtdp: derivatives of transition dipole moment
Procedure evc(m, x_g, x_e, fcg, fce, nacme, dtdp)
! transform the molecule to the inertial reference frame
call transform_to_inertial_reference_frame (m, x_g, x_e, fc_g, fc_e, nacme, dtdp)
! do the Eckart rotation to minimize the vibration-rotation coupling, see Ref. [35]
call eckart_rotation (m, x_g, x_e, fc_g, fc_e, nacme, dtdp)
! Diagonalize the mass-weighted force constant matrix to obtain the frequency and normal mode $\mathbf{C}_g$ and $\mathbf{C}_e$.
call calculate_frequency (m, fc_g, fc_e, C_g, C_e)
! Calculate displacement$\mathbf{D}_g = \mathbf{C}_g^T\mathbf{m}(\mathbf{x}_e - \mathbf{x}_g)$, $\mathbf{D}_e = \mathbf{C}_e^T\mathbf{m}(\mathbf{x}_g - \mathbf{x}_e)$
do $i = 1, 3^*N - 6$ ($3^*N - 5$)
! Loop for normal mode, N is the number of atom
do $j = 1, 3^*N$
! Loop for atom coordinate
$D_g(i) = D_g(i) + C_g(j,i)^* m(j)^* (x_e(j) - x_g(j))$
$D_e(i) = D_e(i) + C_e(j,i)^* m(j)^* (x_g(j) - x_e(j))$
end do
end do
! Calculate Duschinsky rotation matrix $\mathbf{S}_{ge} = \mathbf{C}_g^T\mathbf{C}_e$, $\mathbf{S}_{eg} = \mathbf{C}_e^T\mathbf{C}_g$
do $i = 1, 3^*N - 6$ ($3N - 5$)
! Loop for normal mode, N is the number of atom
do $j = 1, 3^*N - 6$ ($3N - 5$)
do $k = 1, 3^*N$
$S_{ge}(i,j) = S_{ge}(i,j) + C_g(j,k)^* C_e(i,k)$
$S_{eg}(i,j) = S_{eg}(i,j) + C_e(j,k)^* C_g(i,k)$
end do
end do
end do
! project the non-adiabatic coupling matrix from Cartesian coordinate system to normal coordinate system
call proj_nacme()
! project the derivatives of transition dipole moment from Cartesian coordinate system to normal coordinate system
call proj_dip()
end

(2) Absorption, fluorescence spectrum and radiative rate constant calculation part.

E_{ad}: Adiabatic excited energy
S: Duschinsky rotation matrix.
D: mode displacement.
freq: frequency of ground state and excited state.
dtdp: derivatives of transition dipole moment ! For Herzberg-Teller spectra, dtdp is needed.
tdp: transition dipole moment ! For Franck-Condon spectra, tdp is needed.
t_{max}: upper limit of integration time
dt: integration duration of time
Procedure TVCF_Abs_Fluo (E_{ad}, S, D, freq, dtdp, tdp, t_{max}, dt)
$nt = t_{max}/dt$
! This loop is for the calculation of correlation function, and it can parallel by MPI tools
do $it = -nt, nt$
Calculate $\mathbf{A}(it)$, $\mathbf{B}(it)$, $\mathbf{E}(it)$ according to Equations (13)–(15)
Calculate $\mathbf{K}(it)$, $\underline{F}(it)$, $\underline{H}_k^{FC/HT}(it)$, $\mathbf{G}_{kl}^{HT}(it)$ according to Equations (9)–(12)
Calculate $\rho_0^{FC}(it)$, $\rho_k^{FC/HT}(it)$, $\rho_{kl}^{HT}(it)$, $\tilde{\rho}(it)$ according to Equations (6)–(8) and Equation (16)
end do
call FFT ($\tilde{\rho}(it)$) to calculate the spectra function $\sigma(\omega)$ according to Equations (17)–(18)
! Fluorescence radiative rate constant calculation
call fluo_spec_integrate ($\sigma_{ffuo}(\omega)$) according to Equation (19)
End

(3) Internal conversion rate constant calculation part.

nacme: non-adiabatic coupling matrix element
Procedure TVCF_IC (E_{ad}, S, D, freq, nacme, t_{max}, dt)
$nt = t_{max}/dt$
! This loop is for the calculation of correlation function, and it can parallel by MPI tools
do $it = -nt, nt$
Calculate $\mathbf{A}(it)$, $\mathbf{B}(it)$, $\mathbf{E}(it)$ according to Equations (13)–(15)
Calculate $\mathbf{K}(it)$, $\underline{F}(it)$ according to Equations (9)–(12)
Calculate $H_k^{FC/HT}(it)$, $\mathbf{G}_{kl}^{HT}(it)$ according to Ref. [27]
Calculate $\rho_{ic,kl}(it)$ according to Equation (23)
end do
call FFT ($\rho_{ic,kl}(it)$), according to the integration Equation (22) to calculate the internal conversion rate constant k_{ic}.
end

(4) Phosphorescence spectrum, radiative rate and intersystem crossing rate constant calculation part.

The phosphorescence spectrum procedure is the same as the Franck–Condon fluorescence spectra, except for the transition dipole moment between T_1 and S_0 according to Equation (18)
SOC: spin-orbit coupling
dt: integration duration of time
Procedure TVCF_ISC (E_{ad}, S, D, freq, nacme, SOC, t_{max}, dt)
$nt = t_{max}/dt$
! This loop is for the calculation of correlation function, and it can parallel by MPI tools
do $it = -nt, nt$
Calculate $\mathbf{A}(it)$, $\mathbf{B}(it)$, $\mathbf{E}(it)$ according to Equations (13)–(15)
Calculate $\mathbf{K}(it)$, $\underline{F}(it)$ according to Equations (9)–(12)
Calculate $H_k^{FC/HT}(it)$, $\mathbf{G}_{kl}^{HT}(it)$ according to Ref. [28]
Calculate $\rho^{(0)}(it)$ according to Equation (6)
Calculate $\rho_k^{(1)}(it)$ according to Equation (36)
Calculate $\rho_{kl}^{(2)}(it)$ according to Equation (23)
end do
call FFT ($\rho^{(0)}(it)$), according to the integration Equation (33) to calculate the rate constant $k_{isc}^{(0)}$.
call FFT ($\rho_k^{(1)}(it)$), according to the integration Equation (34) to calculate the rate constant $k_{isc}^{(1)}$.
call FFT ($\rho_{kl}^{(2)}(it)$), according to the integration Equation (35) to calculate the rate constant $k_{isc}^{(2)}$.
Calculate k_{isc} according to the integration Equation (29).
end

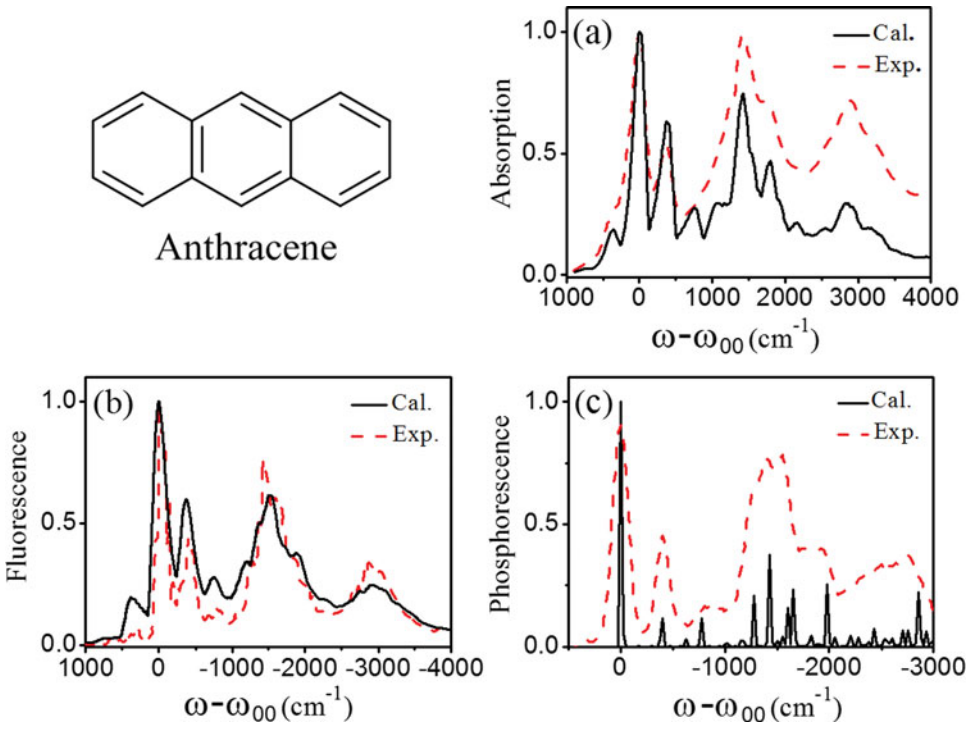

Figure 2. Comparisons between calculated and experimental spectra of anthracene: (a) absorption at 423 K; (b) fluorescence at 433 K; (c) phosphorescence at 77 K.
Source: Reprinted figure with permission from Ref. [36] © 2014, American Chemical Society.

2.5. Example

Here, we take anthracene as an example for the MOMAP's luminescent properties calculation. The equilibrium geometries and vibration frequencies of anthracene in the ground state (S_0) and lowest triplet state are obtained by density functional theory (DFT), and the lowest singlet excited state (S_1) is obtained by time-dependent density functional theory (TDDFT). The non-adiabatic coupling and the spin-orbit coupling are calculated at complete active space self-consistent field (CASSCF) level (for more details on Ref. [4,28]). By importing this electronic structure information into the MOMAP, we get the absorption, fluorescence and phosphorescence spectra, together with the radiative, internal conversion and intersystem crossing rate constants. For better comparison, the spectra are calculated at different temperatures in comparison with the experiment (absorption at 423 K, fluorescence at 433 K and phosphorescence at 77 K) and the spectra are normalised to the maximum intensity. Moreover, the 0-0 transition energies are set to zero. Nice agreements with experimental spectroscopy can be seen in Figure 2 [36]. The calculated rate constants of the radiative decay rate, internal conversion rate and intersystem crossing rate are in good agreement with the previous experimental results, as shown in Table 1.

Table 1. Comparisons between calculated and experimental radiative and internal conversion and intersystem crossing rate constants of anthracene at 298 K.

	k_r	k_{IC}	k_{ISC}	Φ_F
Cal.	2.51×10^7	7.50×10^5	0.26×10^8	0.48
Exp.	6.20×10^{7a}	3.5×10^{5a}	$0.37–0.64 \times 10^{8b}$	~0.4

Note: Unit: s^{-1}.
[a]From Ref. [37].
[b]From Ref. [38].

Another example is the carboxyl substituted polythienylene vinylene, *n*TV-COOH (n = 2–6) [39]. As Figure 3 presented, fluorescence spectrum calculation time via TVCF method scales as N^3, where N is the number of normal modes. All the normal modes and vibrational quantum numbers are included; while with the traditional sum-over-states method, one needs to select important normal modes and give a cut-off for its vibrational quanta. Even so, the computational time scales as $(a + 1)^N$, where a is a the cut-off of vibrational quanta, like the inset of Figure 3 shows. All these examples reveal that the MOMAP can give us an accurate and efficient simulation of the organic materials' luminescent properties.

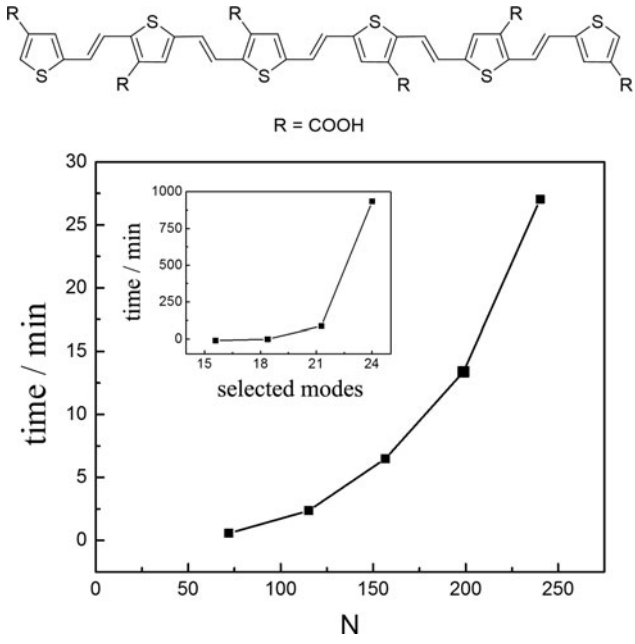

Figure 3. Computing time of fluorescence spectrum versus the number of normal modes (*N*) for *n*TV-COOH (*n* = 2–6) by the TVCF method . The computing time via sum over state method (only two quantum numbers) is shown in the inset.
Source: Reprinted figure with permission from Ref. [39] © 2012, Royal Society of Chemistry.

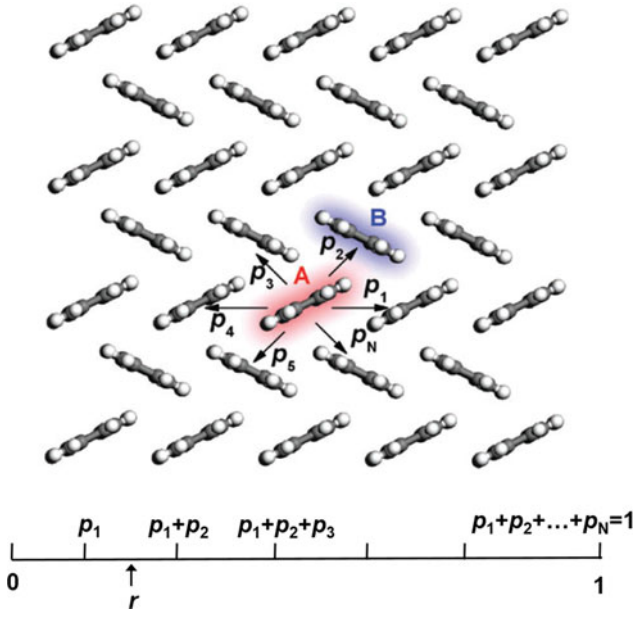

Figure 4. (Top) Schematic representation of the charge hopping pathways from molecule A to its neighbours with the probability p_1, p_2, …, and p_N. (Bottom) A unit length is divided into *N* parts according to each probability. A uniformly distributed random number (*r*) decides which path is chosen for charge hopping, e.g. to molecule B if $p_1 < r < p_1 + p_2$. Thereby, the larger p_2 is, the more probable it is for the charge to go to B.
Source: Reprinted figure with permission from Ref. [31] © 2010, Royal Society of Chemistry.

3. First-principles computation of charge mobility for organic semiconductors

3.1. Charge diffusion simulation through numerical random walk

In order to understand the intrinsic charge transport mechanism, great progress has been achieved to quantitatively analyse the charge mobility by computational chemistry [33]. The charge delocalisation in molecular crystal is dominated by the inter-molecular charge transfer integral *V*, while the intra-molecular reorganisation energy λ characterises the trap effect arising from the electron-vibration coupling. When $\lambda \gg V$, the charge can be regarded as localised, as described by Marcus theory [40]. To better describe transport process within hopping mechanism, we developed a QNT model by considering quantum nature of nuclear motion [30].

The mobility μ in the molecular crystal can be defined as the ratio between the charge drift velocity (υ) and the driving electric field (F) [34]:

$$\mu = \upsilon / F. \tag{37}$$

Within the hopping model, the charge transport process can be characterised by a diffusion process, in which the charge carrier hops between adjacent molecules according to the charge transfer rates that apply in the absence of an external electric field. In the low field limit, the carrier mobility Equation (37) can be described by the Einstein relation in the diffusion limit:

$$\mu = eD/k_{\mathrm{B}}T, \tag{38}$$

where e is the electron charge, D is the charge diffusion coefficient, k_{B} is Boltzmann constant and T is temperature. For an n-dimensional system, D is defined by the ratio between the mean-square displacement and the diffusion time:

$$D = \frac{1}{2n} \lim_{t\to\infty} \frac{\langle r^2 \rangle}{t} \tag{39}$$

$\langle r^2 \rangle$ represents the statistical average of the square of charge displacement and can be obtained numerically from random walk, which is able to simulate the diffusion process of the charge carrier in the presence of crystal anisotropy (shown in Figure 4).

Within this approach, an arbitrary site (molecule m) in the bulk is initially chosen as the starting position for the charge. Then the transport network should be determined by considering the threshold value of the nearest distance between hopping molecules and the

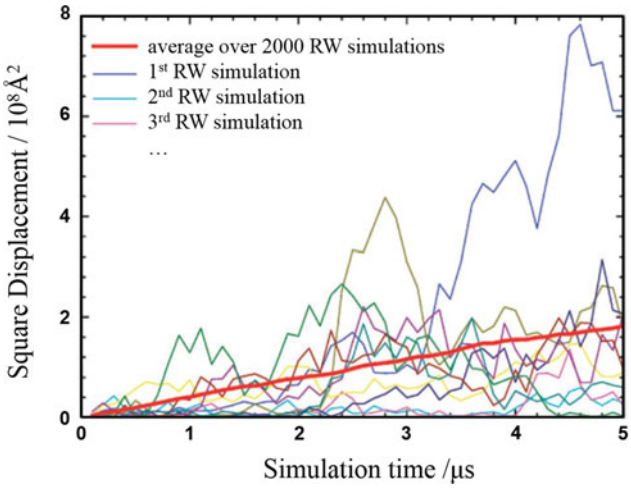

Figure 5. A typical evolution of the square displacement of 10 individual simulations and the mean-square displacement over 2000 simulations.
Source: Reprinted figure with permission from Ref. [31] © 2010, Royal Society of Chemistry.

threshold of the transfer integral V_{mn}. Then the charge transfer rate$k_{ct,mn}$ can be calculated in the framework of quantum tunnelling method, short time approximation (STA) or Marcus equation. In order to determine the next site of the charge in a statistical sense, a random number r that is uniformly distributed between 0 and 1 is generated. If $\sum_{\beta=1}^{\alpha-1} p_\beta^{(m)} < r < \sum_{\beta=1}^{\alpha} p_\beta^{(m)}$, the charge hops to the αth neighbour with a hopping time $\tau_{mn} = 1/k_{\mathrm{ct},mn}$, which assumes no correlation between the hopping events along different paths. The simulation continues until the diffusion distance exceeds the lattice constant by at least 2–3 orders of magnitude. This process is repeated thousands of times and averaged out to get a linear relationship between mean-square displacement and simulation time shown in Figure 5. The mobility is finally evaluated by the Einstein relation (Equation (38)).

3.2. Inter-molecular charge transfer rate with QNT effect

Several methods have been proposed to evaluate the transfer integral for a molecular dimer. The simplest way is the frontier orbital energy level splitting method, in which the transfer integral between identical molecular orbitals of two isolated molecules corresponds to half of the energy level splitting when they form a dimer. The MOMAP V1.0 calculates it with the site-energy overlap correction method [41].

$$V_{mn}^0 = \langle \psi_m | F | \psi_n \rangle \tag{40}$$

where ψ_m and ψ_n are the frontier orbitals of the two isolated molecules m and n in the dimer. Namely, for hole (electron) transport, the highest occupied (lowest unoccupied) molecular oribital, HOMO (LUMO), should be plugged in. Since the orbitals ψ_m and ψ_n are non-orthogonal, the transfer integral can be modified through orthogonalisation process [34],

$$V_{mn} = \frac{V_{mn}^0 - \frac{1}{2}(\varepsilon_m + \varepsilon_n) S_{mn}}{1 - S_{mn}^2} \tag{41}$$

where $\varepsilon_{m(n)}$ is the electron site energy and S_{mn} is the overlap integral between ψ_m and ψ_n.

The frequency, Huang–Rhys factor, and reorganisation energy between neutral and ionic molecules are calculated using EVC program. The general quantum-mechanical CT rate was derived by Jortner and Lin *et al.* [42–44]. Starting from Fermi's golden rule and within the framework of the displaced oscillator approximation, the charge transfer rate with QNT effects can be represented as

$$k_{\mathrm{ct},mn}^{\mathrm{QNT}} = \frac{|V_{mn}|^2}{\hbar^2} \int_{-\infty}^{\infty} \mathrm{d}t \exp\left\{ i\omega_{fi} t - \sum_j S_j \left[(2\bar{n}_j + 1) - \bar{n}_j e^{-i\omega_j t} - (\bar{n}_j + 1) e^{i\omega_j t} \right] \right\} \tag{42}$$

Here, $\omega_{fi} = (E_f - E_i)/\hbar$ is adiabatic energy between initial state ($D^{\pm}A$) and final state ($DA^{\pm}$). S_j is the Huang–Rhys factor and $\bar{n}_j = 1/(e^{\hbar\omega_j/k_B T} - 1)$ is the occupation number for the jth vibrational normal mode with frequency ω_j. In the strong coupling limit ($\sum_j S_j >> 1$), STA can be applied to guarantee the convergence of the integration of Equation (41). In STA, the mode with the largest Huang–Rhys factor S_k is selected for a Taylor expansion: $e^{\pm i\omega t} \approx 1 \pm i\omega t - \omega^2 t^2/2$. Then Equation (42) will be derived as

$$k_{\mathrm{ctmn}}^{\mathrm{STA}} = \frac{|V_{mn}|^2}{\hbar^2} \int_{-\infty}^{\infty} \mathrm{d}t \exp\left\{ i(\omega_{fi} + S_k\omega_k) t - S_k \left(\bar{n}_k + \frac{1}{2}\right) \omega_k^2 t^2 \right\} \times \exp\left\{ -\sum\nolimits_{j(\neq k)} S_j \left[(2\bar{n}_j + 1) - \bar{n}_j e^{-i\omega_j t} - (\bar{n}_j + 1) e^{i\omega_j t} \right] \right\} \tag{43}$$

If STA is applied to all modes, and considering the classical regime – that is high temperature, low frequency regime where $\hbar\omega_j/k_B T << 1$, and then $\bar{n}_j \approx k_B T/\hbar\omega_j$, Equation (43) reduces to Marcus equation,

$$k_{\mathrm{ct},mn}^{\mathrm{Marcus}} = \frac{|V_{mn}|^2}{\hbar^2} \sqrt{\frac{\hbar^2\pi}{\lambda k_B T}} \exp\left\{ -\frac{(\Delta G_{fi} + \lambda)^2}{4\lambda k_B T} \right\} \tag{44}$$

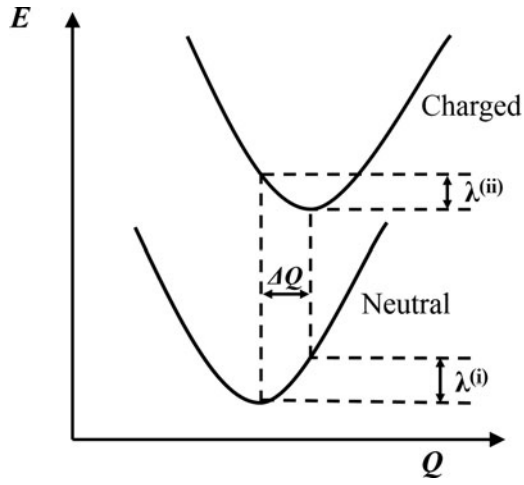

Figure 6. Schematic representation of the potential energy surfaces of the neutral and charged molecules with respect to the reaction coordinate. The sum of the two relaxation energies $\lambda^{(i)}$ and $\lambda^{(ii)}$ is the internal reorganisation energy.
Source: Reprinted figure with permission from Ref. [31] © 2010, Royal Society of Chemistry.

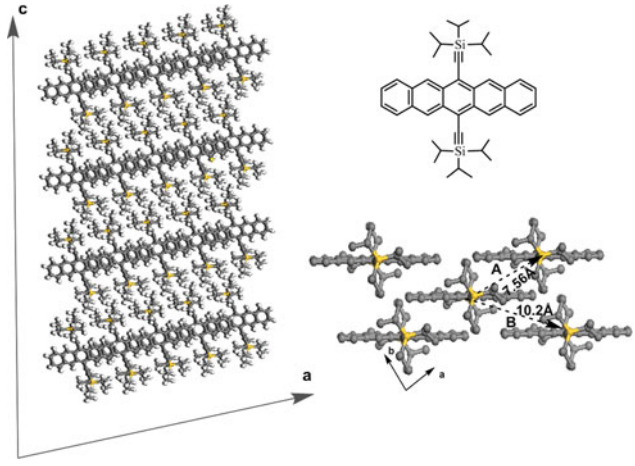

Figure 7. (Left) A $5 \times 5 \times 3$ supercell structure of a TIPS-pentacene crystal of thin film phase. (Right top) Molecular structure and (right bottom) an *ab* plane structure extracted from the supercell. Two pairs of molecules are indicated as dimer A and B.
Source: Reprinted figure with permission from Ref. [34] © 2012, Wiley-VCH.

where $\Delta G_{fi} = E_f - E_i = \hbar\omega_{fi}$. and $\lambda = \lambda^{(i)} + \lambda^{(ii)}$ is the total reorganisation energy for molecule m and n; see Figure 6. $k_{ct,mn}^{QNT}$, $k_{ct,mn}^{STA}$, $k_{ct,mn}^{Marcus}$, can be obtained in MOMAP separately, and here all denoted as $k_{ct,mn}$ for simplicity. For molecule m, the hopping probability to molecule n ($\neq m$) can be represented as

$$p_n^{(m)} = \frac{k_{ct,mn}}{\sum_{n\in\{\text{neighbors of } m\}} k_{ct,mn}} \tag{45}$$

3.3. Algorithm

The program algorithms of charge mobility are listed below, including the preparation of molecular structure part; search neighbour part; transfer integral calculation part; reorganisation energy calculation part; hopping rate and probability calculation part; random walk simulation part; diffusion constant and mobility calculation part.

(1) The preparation of molecular structure file part

```
procedure separate_molecule()
   ! Read molecular crystal structure file in CIF (Crystallographic
Information File) format. Separate each single molecule from the unit
cell and save as mol1.mol, mol2.mol, ….
   call separate_mol (cif_file)
end
```

(2) Search neighbour part

```
procedure find_neighbour(mol1.com, mol2.com, …, lat_cutoff)
   ! For each molecule in the unit cell, find its transport neighbours
within the neighbour distance cutoff.
   ! n_mol: number of molecules
   do i = 1, n_mol
      call find_neighbour(lat_cutoff)
   end do
end
```

(3) Transfer integral calculation part

```
procedure transfer_integral()
do i = 1, n_mol
      ! n_neigbour: number of neigbours for molecule i.
      do j = 1, n_neigbour
      ! Calculate the transfer_integral between molecule i and molecule j
according to Equation (41).
      call calculate_transferintegral (i, j)
      end do
   end do
end
```

(4) Calculate reorganisation energy using evc module

```
m: molecular mass
x_n: molecular coordinate of neutral state
x_i: molecular coordinate of ionic state
fc_n: molecular force constant of neutral state
fc_i: molecular force constant of ionic state
Procedure evc (m, x_n, x_i, fc_n, fc_i)
   ! transform the molecule to the inertial reference frame
   call transform_to_inertial_reference_frame (m, x_n, x_i, fc_n, fc_i)
   ! do the Eckart rotation to minimize the vibration-rotation coupling,
see Ref [35]
   call eckart_rotation (m, x_n, x_i, fc_n, fc_i)
   ! Diagonalize the mass-weighted force constant matrix to obtain the
frequency and normal mode C_n and C_i.
   call calculate_frequency (m, fc_n, fc_i, C_n, C_i)
   ! Calculate displacement D_n = C_n^T m(x_i − x_n), D_i = C_i^T m(x_n − x_i)
   do i = 1, 3 * N − 6 (3 * N − 5)
   ! Loop for normal mode, N is the number of atom
      do j = 1, 3 * N
      ! Loop for atom coordinate
         D_n(i) = D_n(i) + C_n(j, i) * m(j) * (x_i(j) − x_n(j))
         D_i(i) = D_i(i) + C_i(j, i) * m(j) * (x_n(j) − x_i(j))
      end do
   end do
end
```

(5) Hopping rate and probability calculation part.

```
V: transfer integral
ω: frequency
HRF: Huang–Rhys factor
procedure hoprate (V, ω, HRF)
   do i = 1, n_mol
      do j = 1, n_neigbour
         ! Calculate the hopping rate and hopping probability between
molecule i and molecule j according to quantum nuclear tunneling
Equation (42) or Marcus equation Equation (44).
         call calculate_hopping_rate (i, j)
         call calculate_hopping_probability(i, j) ! according to Equation
(45)
      end do
   end do
end
```

(6) Random walk simulation part.

```
procedure random_walk()
   ! nt: number of time step
   do it = 1, nt
      call random_r(r)
      ! According to Figure 4, decide which molecule to hop.
      i = this_molecule
      call hopping_to_molecule (r, i, j)
time(it) = time(it ,k − 1) + 1/rate (i, j)
      x(it) = x(it − 1) + dx(i, j)
if (time(it) ≥ time_max) then
         exit
      end if
   end do
end
```

(7) Diffusion constant and mobility calculation part.

```
procedure calculate_mobility()
   ! Calculate diffusion constant according to Equation (39)
   call calculate_diffusion_constant()
   ! Calculate mobility according to Equation (38)
   call calculate_mobility()
end
```

3.4. Example

TIPS-pentacene crystal is taken as an example [34] to demonstrate the calculation of hole mobility with MOMAP. Molecular structure and crystal packing for TIPS-P [45] are shown in Figure 7. The transfer integral V is calculated for all the neighbouring molecular pairs. The neutral and cation molecules are optimised by DFT and unrestricted DFT for singly charged state, with a BhandHLYP functional and a 6-31G(d) basis set, respectively. Then the vibration frequencies are calculated at the corresponding equilibrium geometries. The frequency, Huang–Rhys factors and reorganisation energy can be obtained from the EVC module. The reorganisation energy for each mode (electron–phonon coupling) is depicted in Figure 8. The total reorganisation energy from the summation of all normal modes is 217 meV, close to 222 meV calculated from full geometry

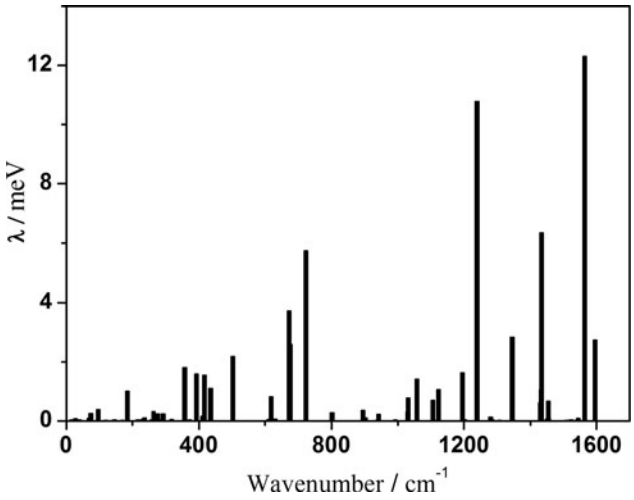

Figure 8. Contribution of the normal modes to the charge reorganisation energy $\lambda^{(1)}$, which is the relaxation energy for singly positively charged molecule from the equilibrium structure of the neutral molecule.
Source: Reprinted figure with permission from Ref. [34] © 2012, Wiley-VCH.

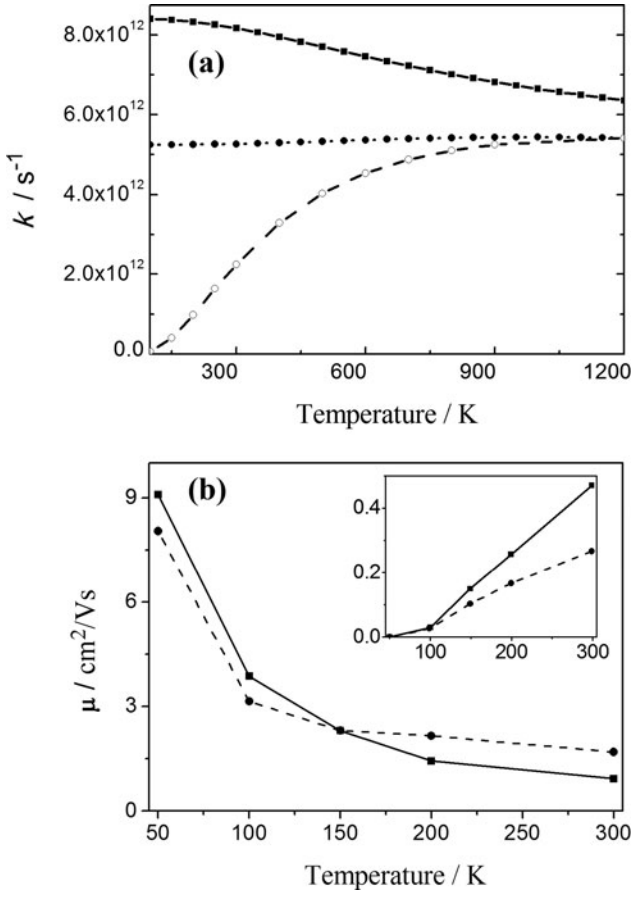

Figure 9. (a) Hole transfer rates (k) for dimer A: filled squares for full quantum rate, filled circles for quantum rate with short time approximation and open circles for semi-classical Marcus theory. (b) Hole mobility and the classical Marcus rate result in the inset.
Source: Reprinted figure with permission from Ref. [34] © 2012, Wiley-VCH.

optimisation, indicating that the harmonic oscillator approximation is valid for this rigid molecule.

The summation of Huang–Rhys factor $\sum_j S_j = 1.97$, which means $\sum_j S_j >> 1$ is not fully satisfied. Then the STA is not a good approximation for this system. From Figure 9(a), we can see that the quantum rate is insensitive and slightly decreases with T at higher temperature, while the semi-classical Marcus charge transfer (CT) rate increases with T, and tends to the limitation of STA result. The quantum CT rate with STA deviates from the full quantum rate even at high temperature. It is found that the semi-classical Marcus rate approaches the quantum rate with STA around $T \sim 1000$ K, indicating that the high temperature approximation is not valid for organic semiconductors at room temperature. Figure 9(b) shows that the dependence of mobility on temperature with QNT gives a $d\mu/dT < 0$ band-like behaviour for localised charge in TIPS-P, which is in sharp contrast to Marcus theory (the inset in Figure 9(b)). It is precisely the phonon-assisted current mechanism. The hole mobility at room temperature is calculated to be 1.7 $cm^2\ V^{-1}\ s^{-1}$, very close to 1.5 $cm^2\ V^{-1}\ s^{-1}$ of the experiment observation [46]. Such good agreement indicates the validity and power of MOMAP for mobility prediction and molecular design.

4. Concluding remarks

Computational quantum chemistry is playing a more and more important role for molecular design of organic functional materials. In this paper, we have first introduced the MOMAP V1.0 as an accurate and effective tool to simulate the organic molecular optical spectra (absorption, fluorescence, phosphorescence) and rate constants (radiative, internal conversion, intersystem crossing) as well as the charge mobility for organic semiconductors. In particular, MOMAP has been used in understanding various luminescent phenomena, such as AIE [8,18,19], TADF [12,13] and room temperature phosphorescence [47,48]. Next generation of MOMAP will focus on more other characteristics of the organic photoelectric materials, like the photocurrent-voltage of the organic solar cell. We hope MOMAP can offer a promising avenue for the photoelectric materials' development.

Disclosure statement

No potential conflict of interest was reported by the authors.

Funding

The work has been supported by the Ministry of Science and Technology of China [grant number 2017YFA0204501], [grant number 2015CB65502]; National Natural Science Foundation of China [grant number 91622121], [grant number 91333202], [grant number 21290191]; Strategic Priority Research Program of the Chinese Academy of Sciences [grant number XDB12020200].

References

[1] *Materials Genome Initiative for Global Competitiveness* (Executive Office of the President of the United States, Washington, DC, 2011).
[2] J. Mei, N.L.C. Leung, R.T.K. Kwok, J.W.Y. Lam, and B.Z. Tang, Chem. Rev. **115**, 11718 (2015).
[3] Q. Peng, Y. Yi, Z. Shuai, and J. Shao, J. Chem. Phys. **126**, 114302 (2007).
[4] Q. Peng, Y. Niu, Q. Shi, X. Gao, and Z. Shuai, J. Chem. Theory Comput. **9**, 1132 (2013).
[5] Z. Shuai and Q. Peng, Natl. Sci. Rev. **4**, 224 (2017).
[6] Q. Wu, C. Deng, Q. Peng, Y. Niu, and Z. Shuai, J. Comput. Chem. **33**, 1862 (2012).
[7] T. Zhang, H. Ma, Y. Niu, W. Li, D. Wang, Q. Peng, Z. Shuai, and W. Liang, J. Phys. Chem. C **119**, 5040 (2015).
[8] T. Zhang, Q. Peng, C. Quan, H. Nie, Y. Niu, Y. Xie, Z. Zhao, B.Z. Tang, and Z. Shuai, Chem. Sci. **7**, 5573 (2016).
[9] Q. Shi, Q. Peng, S. Sun, and Z. Shuai, Acta Chim. Sin. **71**, 884 (2013).
[10] Q. Peng, Q. Shi, Y. Niu, Y. Yi, S. Sun, W. Li, and Z. Shuai, J. Mater. Chem. C **4**, 6829 (2016).
[11] H. Uoyama, K. Goushi, K. Shizu, H. Nomura, and C. Adachi, Nature **492**, 234 (2012).
[12] Q. Peng, D. Fan, R. Duan, Y. Yi, Y. Niu, D. Wang, and Z. Shuai, J. Phys. Chem. C **121**, 13448 (2017).
[13] L. Lin, Z. Wang, J. Fan, and C. Wang, Org. Electron. **41**, 17 (2017).
[14] J.-L. Brédas, D. Beljonne, and V. Coropceanu, J. Cornil, Chem. Rev. **104**, 4971 (2004).
[15] X. Yang, L. Wang, C. Wang, W. Long, and Z. Shuai, Chem. Mater. **20**, 3205 (2008).
[16] G. Nan, X. Yang, L. Wang, Z. Shuai, and Y. Zhao, Phys. Rev. B **79**, 115203 (2009).
[17] L. Tang, M. Long, D. Wang, and Z. Shuai, Sci. China Ser. B **52**, 1646 (2009).
[18] T. Zhang, Y. Jiang, Y. Niu, D. Wang, Q. Peng, and Z. Shuai, J. Phys. Chem. A **118**, 9094 (2014).
[19] W. Li, Q. Peng, Y. Xie, T. Zhang, and Z. Shuai, Acta Chim. Sin. **74**, 902 (2016).
[20] Y. Jiang, X. Zhong, W. Shi, Q. Peng, H. Geng, Y. Zhao, and Z. Shuai, Nanoscale Horiz. **1**, 53 (2016).
[21] Z. Ma, H. Geng, D. Wang, and Z. Shuai, J. Mater. Chem. C **4**, 4546 (2016).
[22] S.G. Chiodo and T. Mineva, J. Chem. Phys. **142**, 114311 (2015).
[23] Z. Zhao, J. Hao, X. Song, S. Ren, and C. Hao, RSC Adv. **5**, 49752 (2015).
[24] D. Escudero, Acc. Chem. Res. **49**, 1816 (2016).
[25] Z. Shuai and Q. Peng, Phys. Rep. **537**, 123 (2014).
[26] Q. Peng, Y. Yi, Z. Shuai, and J. Shao, J. Am. Chem. Soc. **129**, 9333 (2007).
[27] Y. Niu, Q. Peng, and Z. Shuai, Sci. China Ser. B **51**, 1153 (2008).
[28] Y. Niu, Q. Peng, C. Deng, X. Gao, and Z. Shuai, J. Phys. Chem. A **114**, 7817 (2010).

[29] Z. Shuai, H. Geng, W. Xu, Y. Liao, and J.-M. Andre, Chem. Soc. Rev. **43**, 2662 (2014).
[30] G. Nan, X. Yang, L. Wang, Z. Shuai, and Y. Zhao, Phys. Rev. B **79**, 115203 (2009).
[31] L. Wang, G. Nan, X. Yang, Q. Peng, Q. Li, and Z. Shuai, Chem. Soc. Rev. **39**, 423 (2010).
[32] L. Wang, G.M. Rangger, Z. Ma, Q. Li, Z. Shuai, E. Zojer, and G. Heimel, Phys. Chem. Chem. Phys. **12**, 4287 (2010).
[33] Z. Shuai, L. Wang, and Q. Li, Adv. Mater. **23**, 1145 (2011).
[34] H. Geng, Q. Peng, L. Wang, H. Li, Y. Liao, Z. Ma, and Z. Shuai, Adv. Mater. **24**, 3568 (2012).
[35] A.Y. Dymarsky and K.N. Kudin, J. Chem. Phys. **122**, 124103 (2005).
[36] Z. Shuai, D. Wang, Q. Peng, and H. Geng, Acc. Chem. Res. **47**, 3301 (2014).
[37] N. Nijegorodov, V. Ramachandran, and D.P. Winkoun, Spectrochim. Acta A **53**, 1813 (1997).
[38] E.A. Gastilovich, V.G. Klimenko, N.V. Korol'kova, R.N. Nurmukhametov, and S.A. Serov, Opt. Spectrosc. **105**, 38 (2008).
[39] Y. Jiang, Q. Peng, X. Gao, Z. Shuai, Y. Niu, and S.H. Lin, J. Mater. Chem. **22**, 4491 (2012).
[40] A.N. Sokolov, S. Atahan-Evrenk, R. Mondal, H.B. Akkerman, R.S. Sánchez-Carrera, S. Granados-Focil, J. Schrier, S.C.B. Mannsfeld, A.P. Zoombelt, Z. Bao, and A. Aspuru-Guzik. Nat. Commun. **2**, 437 (2011).
[41] E.F. Valeev, V. Coropceanu, D.A. da Silva Filho, S. Salman, and J.-L. Brédas, J. Am. Chem. Soc. **128**, 9882 (2006).
[42] J. Ulstrup and J. Jortner, J. Chem. Phys. **63**, 4358 (1975).
[43] J. Jortner, J. Chem. Phys. **64**, 4860 (1976).
[44] S.H. Lin, C.H. Chang, K.K. Liang, R. Chang, Y.J. Shiu, J.M. Zhang, T.S. Yang, M. Hayashi, and F.C. Hsu, Adv. Chem. Phys. **121**, 1 (2002).
[45] J.E. Anthony, J.S. Brooks, D.L. Eaton, and S.R. Parkin, J. Am. Chem. Soc. **123**, 9482 (2001).
[46] D. Emin and T. Holstein, Ann. Phys. **53**, 439 (1969).
[47] Z. He, W. Zhao, J.W.Y. Lam, Q. Peng, H. Ma, G. Liang, Z. Shuai, and B.Z. Tang, Nat. Commun. **8**, 416 (2017).
[48] H. Ma, W. Shi, J. Ren, W. Li, Q. Peng, and Z. Shuai, J. Phys. Chem. Lett. **7**, 2893 (2016).